The Astrophysical Journal Letters, 735:L11 (5pp), 2011 July 1 doi:10.1088/2041-8205/735/1/L11

NUCLEAR STAR-FORMING RING OF THE MILKY WAY: SIMULATIONS

Sungsoo S. Kim[1,2,3,8], Takayuki R. Saitoh[4], Myoungwon Jeon[1,5], Donald F. Figer[3], David Merritt[6], and Keiichi Wada[7]
[1] Department of Astronomy & Space Science, Kyung Hee University, Yongin, Kyungki 446-701, Republic of Korea
[2] School of Space Research (WCU program), Kyung Hee University, Yongin, Kyungki 446-701, Republic of Korea
[3] Center for Detectors, Rochester Institute of Technology, Rochester, NY 14623, USA
[4] Center for Computational Astrophysics, National Astronomical Observatory of Japan, Mitaka, Tokyo 181-8588, Japan
[5] Department of Astronomy, University of Texas, Austin, TX 78712, USA
[6] Department of Physics and Center for Computational Relativity and Gravitation, Rochester Institute of Technology, Rochester, NY 14623, USA
[7] Graduate School of Science and Engineering, Kagoshima University, Kagoshima 890-8580, Japan
Received 2011 February 19; accepted 2011 May 19; published 2011 June 6

ABSTRACT

We present hydrodynamic simulations of gas clouds in the central kpc region of the Milky Way that is modeled with a three-dimensional bar potential. Our simulations consider realistic gas cooling and heating, star formation, and supernova feedback. A ring of dense gas clouds forms as a result of X_1–X_2 orbit transfer, and our potential model results in a ring radius of ∼200 pc, which coincides with the extraordinary reservoir of dense molecular clouds in the inner bulge, the Central Molecular Zone (CMZ). The gas clouds accumulated in the CMZ can reach high enough densities to form stars, and with an appropriate choice of simulation parameters, we successfully reproduce the observed gas mass and the star formation rate (SFR) in the CMZ, $\sim 2 \times 10^7\ M_\odot$ and $\sim 0.1\ M_\odot\ \mathrm{yr}^{-1}$. Star formation in our simulations takes place mostly in the outermost X_2 orbits, and the SFR per unit surface area outside the CMZ is much lower. These facts suggest that the inner Galactic bulge may harbor a mild version of the nuclear star-forming rings seen in some external disk galaxies. Furthermore, from the relatively small size of the Milky Way's nuclear bulge, which is thought to be a result of sustained star formation in the CMZ, we infer that the Galactic inner bulge probably had a shallower density profile or stronger bar elongation in the past.

Key words: galaxies: ISM – galaxies: star formation – Galaxy: center – Galaxy: nucleus – ISM: kinematics and dynamics

1. INTRODUCTION

CO emission surveys along the Galactic plane reveal that molecular gas is abundant in the plane down to a Galactocentric radius r of ∼3 kpc (see, e.g., Dame et al. 2001). Inside this radius, the amount of molecular emission greatly reduces, as do star formation activities. However, a significant amount of molecular gas, as well as various evidences of recent star formation, appears again inside r of ∼200 pc (Morris & Serabyn 1996, hereafter MS96; Yusef-Zadeh et al. 2009, hereafter YZ09). This region of abundant molecular gas is called the Central Molecular Zone (CMZ). The total gas mass inside $r = 250$ pc is estimated to be $(1.7–5) \times 10^7\ M_\odot$ (Dahmen et al. 1998; Pierce-Price et al. 2000; Launhardt et al. 2002).

The gas in the CMZ must have migrated inward from the Galactic disk through interactions with other clouds, field stars, and magnetic fields (MS96). A mixed atomic/molecular layer inside $r \simeq 3$ kpc turns into a mostly molecular, high-density medium at the CMZ (Liszt & Burton 1978; MS96). Binney et al. (1991) hypothesize that this abrupt change in gas content and density is caused by a transition between so-called X_1 and X_2 orbits near $r = 200$ pc. X_1 is a family of stable, closed orbits elongated along the bar's major axis, whereas X_2 orbits are elongated along the bar's minor axis, much deeper in the potential (Contopoulos & Papayannopoulos 1980). The spiraling-in gas clouds would generally follow the X_1 orbits until the orbits become sharply cusped and even self-intersecting at the innermost X_1 region. Gas clouds experience compression and shocks near the cusps of these orbits, lose angular momentum, and plunge to the X_2 orbits inside. The infalling gas clouds can additionally lose angular momentum when they collide with those already on the X_2 orbits. This compression and subsequent cooling will transform the gas into molecular form, and the molecular clouds accumulated in the X_2 region would correspond to the CMZ.

The abundance and high densities of molecular gas in the CMZ naturally lead to star formation. Indeed the CMZ harbors two extraordinary, young (few Myr), massive (a few $10^4\ M_\odot$) star clusters, the Arches and the Quintuplet (Figer et al. 1999; Kim et al. 2006, among others) as well as a population of young stellar objects (YZ09). Serabyn & Morris (1996) propose that star formation has been occurring in the CMZ throughout the lifetime of the Galaxy, and the resulting stellar population is evident as the central r^{-2} cluster or the nuclear bulge, a prominent cusp in the stellar density profile, whose extent is similar to that of the CMZ.

There have been a few numerical studies on the hydrodynamics of the gas layer in the Galactic inner bulge. Jenkins & Binney (1994) examined the hypothesis of Binney et al. (1991) with two-dimensional (2D) sticky particle simulations and confirmed that the transition of gas motion from X_1 to X_2 orbits indeed takes place in a bar potential. Lee et al. (1999) and Englmaier & Gerhard (1999) were able to observe the same phenomenon in their 2D smoothed particle hydrodynamics (SPH) simulations. Rodriguez-Fernandez & Combes (2008) performed 2D hydrodynamic simulations (particle motions followed in 3D) with a more sophisticated potential model for the inner Galaxy in an attempt to reproduce the observed velocity structure of the CMZ. All of these studies primarily concentrated on the

[8] A part of S.S.K.'s work was conducted at Rochester Institute of Technology during his sabbatical leave from Kyung Hee University.

behavior of the gas flows and were not able to follow the density and temperature evolution of the gas clouds and subsequent star formation,[9] due to the limits in their numerical schemes and/or computing power at those times.

In the present Letter, we present 3D hydrodynamic simulations for the motions of gas clouds and star formation in the inner bulge of the Galaxy. Our simulations consider self-gravity, gas cooling and heating, and supernova (SN) feedback. We show that a bar potential can indeed compress and cool the gas sufficiently enough to form stars and that the obtained star formation rates (SFRs) are consistent with observations.

2. METHODS AND MODELS

We use a parallel *N*-body/SPH code ASURA (Saitoh et al. 2008, 2009) for our simulations. We use an opening angle of $\theta = 0.5$ for a cell opening and a softening length of 3 pc, and the kernel size of an SPH particle is determined by imposing the number of neighbors to be 32 ± 2. We implement a cooling function by Spaans & Norman (1997) for gas with a solar metallicity for a temperature range of 10–10^8 K, and uniform heating from far-ultraviolet (FUV) radiation is considered. The standard radiation strength used in our simulations is $100\,G_0$,[10] which is ∼60 times the solar neighborhood value (the SFR per unit surface area in the CMZ is ∼60 times larger than that in the solar neighborhood; YZ09). The effect of SN feedback is implemented by supplying thermal energy into the surrounding 32 gas particles.

A star particle is spawned when a gas particle satisfies all of the following four conditions: (1) hydrogen number density is larger than the threshold density, $n_{\rm th}$, (2) temperature is lower than the threshold temperature, $T_{\rm th}$, (3) the flow is converging ($\nabla \cdot \mathbf{v} < 0$), and (4) there is no heat supply from nearby SN explosions. We adopt $n_{\rm th} = 100$ cm^{-3} and $T_{\rm th} = 100$ K as our standard threshold values following Saitoh et al. (2008, 2009), who showed that only such a high density and low temperature threshold can reproduce the structural characteristics of galactic disks. The local SFR is assumed to be proportional to the local gas density divided by the local dynamical time,

$$\frac{d\rho_*}{dt} = C_* \frac{\rho_{\rm gas}}{t_{\rm dyn}}, \quad (1)$$

where C_* is the star formation efficiency (SFE) parameter, and we adopt $C_* = 0.033$ as our standard value following Saitoh et al. A newly spawned star particle is set to have one-third of the original gas particle mass. Detailed discussion on the spawning of star particles and SN feedback is given in Saitoh et al.

Following Zhao et al. (1994), we adopt an $m = 2$ bar with a power-law density profile for the inner Galactic bulge:

$$\rho = \rho_0 \left(\frac{r}{r_0}\right)^{-\alpha} [1 - Y(\theta, \phi)], \quad (2)$$

where

$$Y(\theta, \phi) = -b_{20} P_{20}(\cos\theta) + b_{22} P_{22}(\cos\theta) \cos 2\phi, \quad (3)$$

and P is the associated Legendre function. These are linear combinations of spherical harmonic functions of the $l = 2, m =$ 0,2 modes. b_{20} determines the degree of oblateness/prolateness while b_{22} determines the degree of non-axisymmetry. Our standard simulation (simulation 1) has the following parameters: $\alpha = 1.75$, $b_{20} = 0.3$, $b_{22} = 0.1$, $\rho_0 = 40\,M_\odot$ pc^{-3}, $r_0 = 100$ pc, and a bar pattern speed of 63 km s^{-1} kpc^{-1}. This set of parameters gives a bar axis ratio of 1:0.74:0.65 for the isodensity surface that intersects points [$x = 0$, $y = \pm 200$ pc, $z = 0$], an X_1–X_2 transition at $r \sim 200$ pc, inner Lindblad resonance at 660 pc, and a corotation radius of 2.8 kpc. Enclosed masses inside 200 pc and 1000 pc are $10^9\,M_\odot$ and $7 \times 10^9\,M_\odot$, respectively.

Our simulations initially have gas particles only, which are distributed on X_1 orbits whose semi-minor axes range from 300 to 1200 pc. The number of particles on each orbit is proportional to the length of the orbit, and on a given orbit, particles are distributed over the same time interval. The initial vertical distribution of the gas particles follows a Gaussian function with a scale height of 40 pc. Our standard simulation has 2×10^5 gas particles and a total gas mass of $10^8\,M_\odot$, thus each gas particle initially has a mass of $500\,M_\odot$ (the latter is true for all of simulations, thus star particles in our simulations typically have $\sim 170\,M_\odot$). The initial velocities in the plane follow the motions on the X_1 orbits, while the vertical component is initially set to zero. We evolve such initial setup without cooling, heating, star formation, and SN feedback for the first 50 Myr to obtain a hydrodynamically relaxed particle distribution.

3. RESULTS

Three snapshots of our standard simulation are presented in Figure 1 for $T = 0$, 150, and 500 Myr. The sense of galactic rotation in the snapshots is clockwise. The middle panel ($T = 150$ Myr) shows that gas particles near [$x = 0$, $y = \pm 1250$ pc] quickly undergo shocks and compressed clouds plunge to the X_2 orbits along the "dust lanes" in the leading inner edges of the X_1 orbits. The gas accumulated on the X_2 orbits, i.e., the CMZ, initially forms an elongated ring of clouds at $r \sim 200$ pc. The masses of gas clumps and streams in the CMZ of our simulations, 10^5–$10^6\,M_\odot$, agree with those estimated for some clumps from radio observations (e.g., Stark et al. 1991). Gas density is the highest in this ring, and this is where star formation is the most active.

The right panel ($T = 500$ Myr) shows that as the gas infall and star formation in the nuclear ring continue, the radial distribution of gas and stars in the X_2 region broadens (mostly inward[11]). However, star formation still takes place mostly near $r \sim 200$ pc, because newly infalling gas from the dust lanes collides the existing nuclear ring of gas at its outer rim. We note that only ∼15% of the gas flowing down the dust lanes directly enters the CMZ, while the rest flows back to the X_1 region. This fraction is consistent with that found in Regan et al. (1997; 10%–25%).

Evolutions of gas, stellar, and total masses on X_1 and X_2 orbits are shown in Figure 2. The mass transfer from X_1 to X_2 regions takes place quite rapidly between $T \simeq 100$ and ≃200 Myr and then goes into a slower, stable phase (panel (a)). While the total mass in the X_2 region grows nearly constantly after $T = 200$ Myr, the gas mass in the X_2 region, $M_{g,X2}$, is held at a nearly constant value and then decreases very slowly (panel (b)). This implies that star formation in the X_2 region becomes

[9] A recent Milky Way simulation by Baba et al. (2010), whose main interest was gas kinematics, does follow thermal evolution and star formation of the gas.

[10] $G_0 \equiv 1.6 \times 10^{-3}$ erg cm^{-2} s^{-1} is the Habing field (Habing 1968).

[11] The gas particles in the CMZ lose orbital energy via shear viscosity from differential rotation and gradually migrate inward. Some particles should gain angular momentum and the CMZ should broadens outward as well, but those particles would merge with the part of the dust lane stream that returns back to the X_1 region.

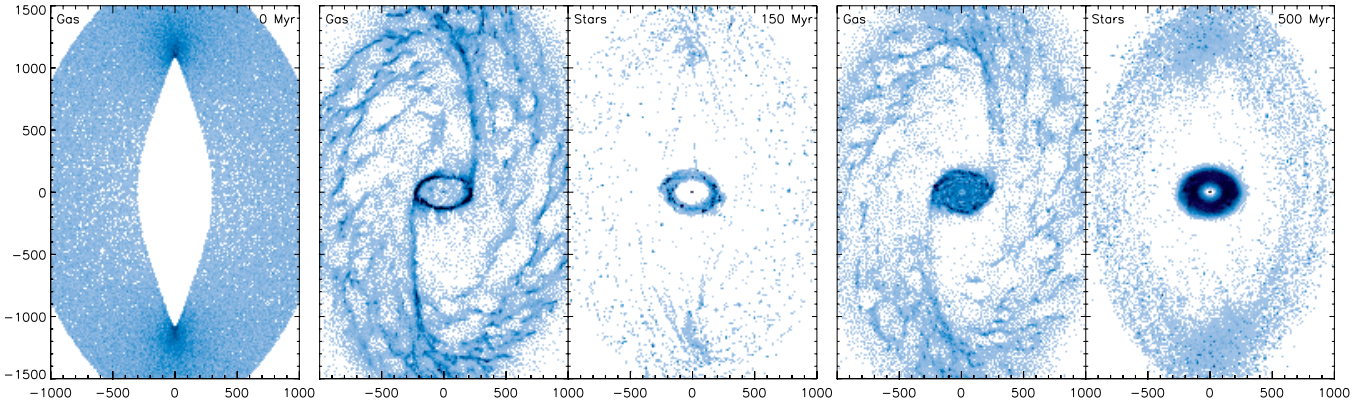

Figure 1. Surface density maps of gas and (accumulated) star particles in simulation 1 at $T = 0$, 150, and 500 Myr. Length units are in parsecs, and the gray scale represents densities linearly from 3 to 300 $M_\odot$ pc^{-2}. The major axis of the bar potential is aligned along the y-axis.

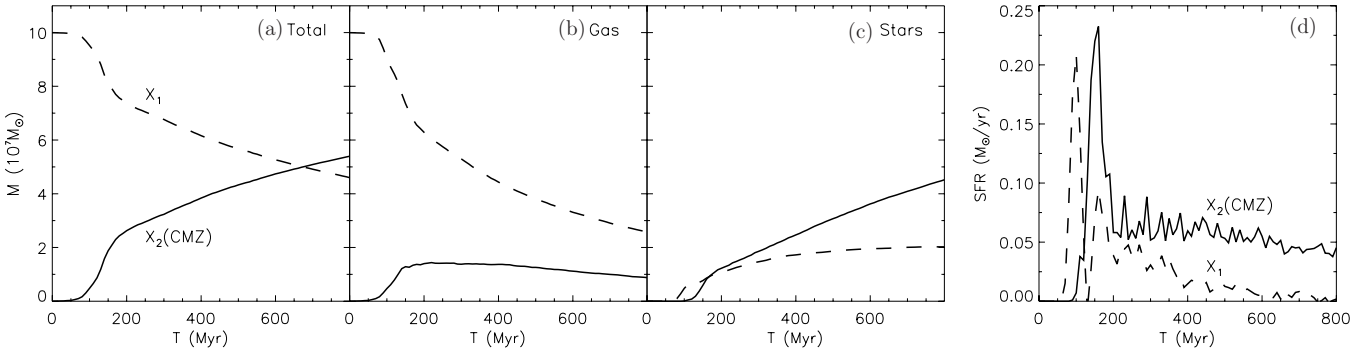

Figure 2. Evolution of total (gas and stars), gas, and stellar masses (panels (a) through (c)), and the star formation rate (panel (d)) in the X_1 (dashed lines) and X_2 (solid lines) regions of simulation 1. After the initial relaxation period ($T > 200$ Myr), most of star formation takes place in the X_2 region (CMZ), and the obtained SFR in the CMZ is consistent with the observed values by YZ09, 0.01–0.1 $M_\odot$ yr^{-1}.

so efficient that all of the newly supplied gas turns into stars once the gas mass in the X_2 region reaches a certain critical value ($\sim 1.5 \times 10^7\ M_\odot$) at $\simeq$200 Myr.

Both the X_1 and X_2 regions initially ($T < 200$ Myr) have high SFRs (see panel (d)), but this is because when the star formation takes place for the first time ($T = 50$ Myr for the X_1 region, $\simeq$100 Myr for the X_2 region), there is no or not enough SN feedback that regulates star formation. Thus, this initial relaxation period should be disregarded if one assumes a continuous gas supply from the outer region (an intermittent gas supply may result in a repetition of a brief, high-SFR phase followed by a longer, lower-SFR phase). While the SFR in the X_1 region continuously decreases as the amount of gas there becomes depleted, the SFR in the X_2 region becomes quite stationary after the initial relaxation period, and ranges between 0.04 and 0.09 $M_\odot$ yr^{-1}. This range is in excellent agreement with recent SFRs estimated for the CMZ from mid-infrared observations by YZ09, 0.01–0.1 $M_\odot$ yr^{-1}.

Simulation 1 clearly shows that (1) under a bar potential modeled for the inner bulge of the Milky Way, gas inflow along the Galactic plane leads to the formation of a gas ring, whose radial extent is consistent with the CMZ, and (2) the gas ring has high enough densities to form stars at a rate consistent with observed values. The parameters of our potential model (ρ_0, r_0, α, b_{20}, and b_{22}) were chosen such that the transition between X_1 and X_2 orbits appears at $\sim$200 pc, therefore the extent of the gas ring in our simulation is a result of the potential parameters that we chose.

On the other hand, it is reasonable to expect that the SFR in the CMZ is determined by the gas influx rate from the X_1 to X_2 regions, and that this influx rate is dependent on the initial gas surface density (or initial gas mass) in the X_1 region. The fact that the SFR from simulation 1 is consistent with the observed values implies that the adopted initial gas mass in our X_1 region (major axes from 300 to 1200 pc) properly reproduces the actual gas influx rate from the X_1 to X_2 regions in the GC.

However, the average $M_{g,X2}$ after relaxation ($200 < T < 600$ Myr) in simulation 1, $1.3 \times 10^7\ M_\odot$, is 20% to four times smaller than the estimated $M_{g,X2}$ values from various observations, $(1.7\text{–}5) \times 10^7\ M_\odot$ (the largest mass estimate is derived from dust emission and is sensitive to the assumed dust temperature in the GC, while the smallest estimate is obtained from C^{18}O molecular line emission; see Section 1 for references).

To see the dependence of $M_{g,X2}$ on initial $M_{g,X1}$, we performed simulation 2, which starts with a twice as large initial $M_{g,X1}$ than simulation 1. Simulation 2 indeed results in $\sim$2 times larger SFRs than simulation 1 as expected, and $\sim$1.5 times larger $M_{g,X2}$ (see Table 1). Now, not only the SFR but also $M_{g,X2}$ is consistent with observations. Note that the CMZ mass is not as sensitive to the gas influx rate as the SFR is.

Simulation 3, whose SFE parameter (C_*) is 10 times smaller than simulation 1 in consideration of the extreme star formation environment in the GC such as strong tidal forces/magnetic fields and elevated gas temperatures, shows another way to increase $M_{g,X2}$—it gives $\sim$25% smaller SFR, but $\sim$40% larger $M_{g,X2}$ ($1.9 \times 10^7\ M_\odot$) than simulation 1. The increase in $M_{g,X2}$ is due to the fact that the star formation in the CMZ now requires higher gas densities than in simulation 1 to compensate for the lowered C_* in Equation (1). From our experiments with

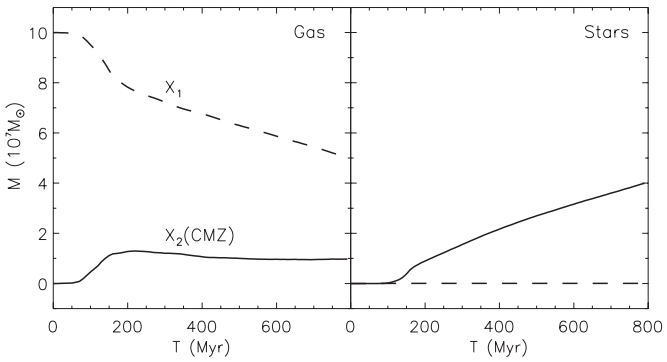

Figure 3. Evolution of gas and stellar masses in the X_1 (dashed lines) and X_2 (solid lines) regions of simulation 4. The increased G_0 effectively suppresses star formation in the X_1 region, where the gas density is lower.

Table 1
Simulation Parameters and Results

Sim	$M_{g,i}$ ($10^7\,M_\odot$)	C_*	$I_{\rm FUV}$ (G_0)	$M_{g,X2}$ ($10^7\,M_\odot$)	$\rm SFR_{X2}$ ($M_\odot\,\rm yr^{-1}$)
1	10	0.033	100	1.33	0.060
2	20	0.033	100	2.03	0.116
3	10	0.0033	100	1.85	0.045
4	10	0.033	1000	1.11	0.057

Notes. $M_{g,i}$ is the initial total gas mass, $I_{\rm FUV}$ is the FUV radiation strength, and $M_{g,X2}$ and $\rm SFR_{X2}$ are the gas mass and the star formation rate in the X_2 region averaged for $T = 200$–600 Myr. The initial number of gas particles is 200,000 for simulations 1, 3, and 4, and 400,000 for simulation 2.

simulations 1 through 3, we conclude that one can fit the observed gas mass and SFR in the CMZ simultaneously by controlling the gas influx rate from the outer bulge (i.e., initial $M_{g,X1}$ in our simulations) and the SFE (C_*).

The actual SFR in the whole X_1 region of the Milky Way is not known yet, as no systematic observations have been made for the region. Simulations 1 through 3 show some star formation in the X_1 region, but it is not possible to accurately calculate steady-state SFRs in the X_1 region from these simulations, because our simulations do not have continuous gas supply from the outer bulge. The total SFRs in the X_1 region of simulations 1 through 3 are only fractions of those in the X_2 region, implying that the SFR per unit volume is much higher in the X_2 region (the volume occupied by the X_1 orbits is ~30 times larger than that occupied by the X_2 orbits in these simulations).

In many nuclear starburst galaxies, star formation takes the form of a ring, i.e., a nuclear star-forming ring. If the Milky Way is such a case, star formation in the inner bulge would be confined in the CMZ and there should be no or very little star formation taking place outside the CMZ. We find from simulation 4 that one way to achieve this is to impose a higher FUV radiation field. Simulation 4, whose G_0 is 10 times larger than simulation 1, gives nearly the same gas mass and SFR in the X_2 region as simulation 1, but almost entirely suppresses star formation in the X_1 region[12] (see Figure 3). It is not certain whether the radiation strength in the inner bulge can actually reach as high as $1000\,G_0$, but other physical mechanisms that can quench star formation in the GC, but are not considered in our simulations, such as strong tidal forces and magnetic fields, may also contribute to the suppression of star formation in the X_1 region as seen in simulation 4.

[12] The suppression of star formation by FUV radiation is much more effective in less dense gas.

Our star formation and SN feedback models successfully reproduce the Kennicutt–Schmidt (K-S) relation. At $T = 400$ Myr, the CMZ in simulation 1 has a gas surface density of $100\,M_\odot\,\rm pc^{-2}$ and a surface SFR of $0.45\,M_\odot\,\rm yr^{-1}\,kpc^2$, the latter of which is 0.45 dex higher than the mean K-S relation, whereas the CMZ in simulation 3 has a surface SFR that is 0.12 dex higher than the mean K-S relation. Considering a rather large scatter in observed SFRs around a mean K-S relation (rms scatter ~0.3 dex; Kennicutt 1998), the SFRs from our simulations are consistent with the K-S relation.

4. THE CMZ AND THE NUCLEAR BULGE

If the star formation in the inner bulge of the Milky Way is indeed confined in the CMZ, and if it has been sustained for the lifetime of the Galaxy as suggested by Figer et al. (2004), the resulting stellar population should manifest in a certain way. Indeed, the infrared intensity profiles in the GC have revealed a prominent, central stellar cusp with an outer extent of about 0.7 deg (~100 pc) on top of the shallower profile made by the Galactic bulge (Serabyn & Morris 1996, and references therein). Serabyn & Morris propose that this "nuclear bulge" is the resulting stellar population from the sustained star formation in the CMZ.[13]

The extent of the nuclear bulge is somewhat smaller than that of the CMZ, and this may indicate that the radius of the CMZ was smaller in the past. From our further simulations with various density slopes (α) and bar elongations (b_{22}), we find that a smaller CMZ radius can be obtained when the density profile is shallower ($\alpha \lesssim 1.6$; the same amount of orbital energy loss at the cusps of X_1 orbits will plunge the gas further inside), or when the bar is more elongated ($b_{22} \gtrsim 0.14$; the gas at the cusps of X_1 orbits will lose larger orbital energy). Therefore, the relatively smaller size of the nuclear bulge may be an important clue on the secular evolution of the Galactic center.

Some of the accumulated gas in the CMZ will keep migrating inward and reach the CircumNuclear Disk (CND) of molecular clouds at $r = 2$–5 pc, and a part of it will sink further to form stars in the central parsec or feed the central supermassive black hole. One possible way to transfer gas from the CMZ to the CND would be a "nested bar," as examined by Namekata et al. (2009).

This work was supported by the Korea Research Foundation (KRF-2008-013-C00037), and by the WCU program (R31-1001) through the NRF funded by the MEST of Korea. We thank the anonymous referee for their valuable comments that greatly improved our Letter. The material in this work is partly supported by NASA under awards NNG 05-GC37G and NNX 10-AF84G, through the Long-Term Space Astrophysics program, and by HPCI Strategic Program Field 5, "The origin of matter and the universe." A part of this research was performed in the Rochester Imaging Detector Laboratory with support from a NYSTAR Faculty Development Program grant.

REFERENCES

Baba, J., Saitoh, T. R., & Wada, K. 2010, PASJ, 62, 1413
Bekki, K. 2010, MNRAS, 401, 2753
Binney, J., Gerhard, O. E., Stark, A. A., Bally, J., & Uchida, K. I. 1991, MNRAS, 252, 210
Contopoulos, G., & Papayannopoulos, T. 1980, A&A, 92, 33

[13] Another way of creating the nuclear bulge is the inspiral of massive star clusters via dynamical friction (Bekki 2010, and references therein).

Dahmen, G., Hüttenmeister, S., Wilson, T. L., & Mauersberger, R. 1998, A&A, 331, 959
Dame, T. M., Hartmann, D., & Thaddeus, P. 2001, ApJ, 547, 792
Englmaier, P., & Gerhard, O. 1999, MNRAS, 304, 512
Figer, D. F., Kim, S. S., Morris, M., Serabyn, E., Rich, R. M., & McLean, I. S. 1999, ApJ, 525, 750
Figer, D. F., Rich, R. M., Kim, S. S., Morris, M., & Serabyn, E. 2004, ApJ, 601, 319
Habing, H. J. 1968, Bull. Astron. Inst. Neth., 19, 421
Jenkins, A., & Binney, J. 1994, MNRAS, 270, 703
Kennicutt, R. C. 1998, ApJ, 498, 541
Kim, S. S., Figer, D. F., Kudrtzki, R. F., & Najarro, F. N. 2006, ApJ, 653, L113
Launhardt, R., Zylka, R., & Mezger, P. G. 2002, A&A, 384, 112
Lee, C. W., Lee, H. M., Ann, H. B., & Kwon, K. H. 1999, ApJ, 513, 242
Liszt, H. S., & Burton, W. B. 1978, ApJ, 226, 790
Morris, M., & Serabyn, E. 1996, ARA&A, 34, 645 (MS96)
Namekata, D., Habe, A., Matsui, H., & Saitoh, T. R. 2009, ApJ, 691, 1525
Pierce-Price, D., et al. 2000, ApJ, 545, L121
Regan, M. W., Vogel, S. N., & Teuben, P. J. 1997, ApJ, 482, L143
Rodriguez-Fernandez, N. J., & Combes, F. 2008, A&A, 489, 115
Saitoh, T. R., Daisaka, H., Kokubo, E., Makino, J., Okamoto, T., Tomisaka, K., Wada, K., & Yoshida, N. 2008, PASJ, 60, 667
Saitoh, T. R., Daisaka, H., Kokubo, E., Makino, J., Okamoto, T., Tomisaka, K., Wada, K., & Yoshida, N. 2009, PASJ, 61, 481
Serabyn, E., & Morris, M. 1996, Nature, 382, 602
Spaans, M., & Norman, C. A. 1997, ApJ, 483, 87
Stark, A. A., Gerhard, O. E., Binney, J., & Bally, J. 1991, MNRAS, 248, 14p
Yusef-Zadeh, F., et al. 2009, ApJ, 702, 178 (YZ09)
Zhao, H., Spergel, D. N., & Rich, R. M. 1994, AJ, 108, 2154